International Journal of Computational Fluid Dynamics, Vol. 20, No. 6, July 2006, 391–400

Taylor & Francis
Taylor & Francis Group

Simulation of flow past a rotating circular cylinder near a plane wall

MING CHENG†*, QIANG YAO†¶ and LI-SHI LUO‡§

†Institute of High Performance Computing, 1 Science Park Road, #01–01, The Capricorn, Singapore Science Park II, Singapore 117528, Singapore
‡Department of Mathematics & Statistics, Old Dominion University, Norfolk, VA 23529, USA

(Received 30 September 2005; in final form 17 May 2006)

A two dimensional incompressible flow past a rotating circular cylinder near a plane wall at $Re = 200$ is investigated by using the lattice Boltzmann equation (LBE). The effects of the gap between the cylinder and the wall, and tangential speed of the cylinder on the frequency of vortex shedding, and the lift and drag forces on the cylinder are quantified together with the flow patterns. With a fixed tangential speed of the cylinder, the flow behavior strongly depends on the normalized cylinder-wall gap $h := H/D$, where H and D are gap height and cylinder diameter, respectively. The flow is steady and behaves almost like a surface mounted object when h is small. With a moderate h, the flow is periodic and pairs of vortices with alternating signs develop due to strong interaction between the rotating cylinder and the wall. As h increases beyond certain value, the wall effect diminishes and the flow behaves almost as in an unbounded domain. Our simulation also validates the LBE method as a tool for direct numerical simulations for hydrodynamics. And we demonstrate that the LBE model with multiple-relaxation-time (MRT) is superior than the popular lattice Bhatnagar–Gross–Krook model in terms of numerical stability and in turn the efficiency.

Keywords: Rotating circular cylinder; Plane wall effect; Unsteady flow; Lattice Boltzmann equation

1. Introduction

The flow past a rotating circular cylinder is a problem of both fundamental and applied interests. When the cylinder rotates in a uniform flow, one half of the cylinder moves along the stream whereas the other moves against. This creates asymmetry in velocity and pressure fields around the rotating cylinder, which in turn lead to asymmetry in the boundary layer separation and a force on the cylinder normal to the flow direction. This phenomenon, referred to as the Magnus effect (Prandtl 1925, Chew *et al.* 1995), has been applied in areas such as ship propulsion and boundary control on airfoil. There exits an extensive literature pertaining to flows around an isolated rotating circular cylinder in a uniform stream, and the flow is now reasonably well understood. However, such is not the case when the cylinder is positioned close to a wall boundary. In the presence of a wall in the flow, the shear effect makes the velocity of approaching stream vary in the direction normal to the cylinder, and the behavior of vortex shedding behind the cylinder is affected. The flow past a rotating cylinder near a plane wall has applications to a number of practical cases in which the flow approaching the cylinder is not uniform but sheared. Examples of such flows are the flow around exposed wheels, such as racing car wheels or airplane landing gears during take-off or landing. Of course, these flows in reality are highly three-dimensional (3D) ones, with the vortex shedding patterns very different from that of the two-dimensional (2D) flows.

It is the intention of this work to investigate the effect of the walls on the flow and the forces experienced by the cylinder. Experiments have shown that the vortex shedding phenomenon of a stationary cylinder near to the wall can be dramatically altered at different gaps between the cylinder and the plane wall (Taneda 1965, Bearman and Zdravkovich 1978, Zdravkovich 1985, Cheng *et al.* 1994, Sumer and Fredsoe 1997, Price *et al.* 2002). The vortex shedding and wade development behind a rotating cylinder near a plane wall have a more complicated stream structure than that of a stationary cylinder, and the flow past a rotating cylinder with or

*Corresponding author. Email: chengm@ihpc.a-star.edu.sg
¶ Email: yaoq@ihpc.a-star.edu.sg
§ Email: lluo@odu.edu

International Journal of Computational Fluid Dynamics
ISSN 1061-8562 print/ISSN 1029-0257 online © 2006 Taylor & Francis
http://www.tandf.co.uk/journals
DOI: 10.1080/10618560601000736

without a wall have different fluid dynamic characteristics. However, there is very little work on the wall effects on the vortex shedding mechanism and wake patterns behind a rotating cylinder near a wall. The study of vortex shedding and wake development behind a rotating cylinder near a wall can help to better understand, for instance, the cause of vortex-induced vibration and its control and suppression.

In this paper, the influence of a plane wall on flow past a 2D rotating circular cylinder in an uniform flow is numerically studied. Specifically, we investigate the effects of the gap H between the cylinder and the wall and the ratio of the tangential velocity U_w to the inflow velocity U, $\gamma := U_w/U$, on the flow. The lattice Boltzmann equation (LBE) with multiple-relaxation-time (MRT) (d'Humières 1992) is used to perform the numerical simulation. The present study will shed some light on the effects of the normalized gap $h = H/D$ and γ on the development of periodic vortex shedding associated with the Kármán vortex street and forces acting on the cylinder. We hope that the results presented in this paper will provide better understanding of the effects of the wall on the vortex shedding mechanism and the structure of wake flow of a rotating cylinder near a wall.

2. Numerical method

The LBE is an alternative to conventional computational fluid dynamics (CFD) methods for solving Navier–Stokes equations (Yu *et al.* 2003). It is based on the Boltzmann equation (or kinetic theory) for the single particle velocity distribution function. Unlike traditional numerical methods, which solve for the macroscopic variables such as velocity and density, the LBE obtains these variables as the moments of the distribution function. As such, the LBE method has some computational advantages because it is based on an equation with a linear advection term—the Boltzmann equation, as opposed to an equation with a nonlinear advection term—the Navier–Stokes equation (van Leer 2001).

2.1 Lattice Boltzmann equation

In what follows, we shall use the generalized lattice Boltzmann equation (GLBE), or the LBE with MRT collision model (d'Humières 1992, Lallemand and Luo 2000, d'Humières *et al.* 2002, Lalemand and Luo 2003). The evolution equation for the MRT–LBE of Q velocities on a D-dimensional lattice $\mathbf{x}_i \in \delta_x \mathbb{Z}^D$ with discrete time $t_n \in \delta_t \mathbb{N}_0 = \delta_t\{0, 1, \dots\}$ is,

$$\begin{aligned}\mathbf{f}(\mathbf{x}_i + \mathbf{c}_i\delta_t, t_n + \delta_t) - \mathbf{f}(\mathbf{x}_i, t_n) &= \boldsymbol{\Omega}(\mathbf{x}_i, t_n) \\ &= -\mathsf{M}^{-1}\cdot\hat{\mathsf{S}}\cdot[\mathbf{m} - \mathbf{m}^{(\mathrm{eq})}],\end{aligned} \tag{1}$$

where M is a $Q \times Q$ matrix which linearly transforms the distribution functions $\mathbf{f} \in \mathbb{V} \equiv \mathbb{R}^Q$ to the velocity moments $\mathbf{m} \in \mathbb{M} \equiv \mathbb{R}^Q$:

$$\mathbf{m} = \mathsf{M}\cdot\mathbf{f}, \quad \mathbf{f} = \mathsf{M}^{-1}\cdot\mathbf{m}, \tag{2}$$

and $\hat{\mathsf{S}}$ a non-negative $Q \times Q$ diagonal relaxation matrix (Lallemand and Luo 2000). The bold-face symbols denote column vectors as the following:

$$\mathbf{f}(\mathbf{x}_i + \mathbf{c}_i\delta_t, t_n + \delta_t) = (f_0(\mathbf{x}_i, t_n + \delta_t), \dots, f_b(\mathbf{x}_i + \mathbf{c}_b\delta_t, t_n + \delta_t))^{\mathrm{T}},$$

$$\mathbf{f}(\mathbf{x}_i, t_n) = (f_0(\mathbf{x}_i, t_n), f_1(\mathbf{x}_i, t_n), \dots, f_b(\mathbf{x}_i, t_n))^{\mathrm{T}},$$

$$\mathbf{m} = (m_0(\mathbf{x}_i, t_n), m_1(\mathbf{x}_i, t_n), \dots, m_b(\mathbf{x}_i, t_n))^{\mathrm{T}},$$

$$\mathbf{m}^{(\mathrm{eq})} = (m_0^{(\mathrm{eq})}(\mathbf{x}_i, t_n), m_1^{(\mathrm{eq})}(\mathbf{x}_i, t_n), \dots, m_b^{(\mathrm{eq})}(\mathbf{x}_i, t_n))^{\mathrm{T}},$$

where T is the transpose operator.

For the sake of simplicity, we will restrict ourselves to the nine-velocity model in 2D (D2Q9 model). The discrete velocities $\{\mathbf{c}_i\}$ are

$$\mathbf{c}_i = \begin{cases} (0,0), & i = 0, \\ (\pm 1, 0)c, (0, \pm 1)c, & i = 1, 2, 3, 4, \\ (\pm 1, \pm 1)c, & i = 5, 6, 7, 8, \end{cases} \tag{3}$$

where $c = \delta_x/\delta_t$. A particular order of moments used here is:

$$\mathbf{m} = (\rho, e, \varepsilon, j_x, q_x, j_y, q_y, p_{xx}, p_{xy})^{\mathrm{T}}, \tag{4}$$

in which ρ is the mass density, and $j_x = \rho u_x$ and $j_y = \rho u_y$ are x and y components of the flow momentum $\mathbf{j}$, respectively, which are the conserved moments in the system. Other moments are non-conserved moments and their equilibria are functions of the conserved moments in the system (d'Humières 1992, Lallemand and Luo 2000, d'Humières *et al.* 2002, Lallemand and Luo 2003). With the above order of moments, the corresponding diagonal relaxation matrix of relaxation rates $\{s_i\}$ is

$$\hat{\mathsf{S}} = \mathsf{diag}\,(s_\rho, s_e, s_\varepsilon, s_\chi, s_q, s_\chi, s_q, s_\nu, s_\nu). \tag{5}$$

In the usual LBE simulations, because ρ, j_x and j_y are conserved quantities, the relaxation rates s_ρ and s_χ have no effect on the system and therefore can assume any value. However, if an external force is in presence, its effect is influenced by the value of s_χ. The relaxation rates s_ν and s_e determine the shear and bulk viscosities, respectively. In the presence of solid boundaries, s_q affects the exact locations where the no-slip boundary conditions are satisfied (Ginzbourg and Adler 1994, Ginzbourg and d'Humières 1996, 2003, Pan *et al.* 2005). The transformation matrix M can be uniquely constructed from the monomials of velocity components $c_{i,\alpha}^n c_{j,\beta}^m \dots c_{k,\gamma}^l$, where α, β and $\gamma \in \{x, y\}$, by

using the Gramd-Schmit orthogonalization procedure (d'Humières 1992, Lallemand and Luo 2000, d'Humières *et al.* 2002). For the D2Q9 model, M can be found in (Lallemand and Luo 2000).

To reduce effect of round-off error, we use the density fluctuation $\delta\rho$ and assume the mean density $\bar{\rho} = 1$. The total density is, therefore, $\rho = \bar{\rho} + \delta\rho$. In addition, we use $\mathbf{j} = \bar{\rho}\mathbf{u}$ to reduce effects due to compressibility (He and Luo 1997). Thus the conserved quantities in an *athermal* LBE model and the corresponding equilibria are:

$$\begin{aligned} \delta\rho^{(\mathrm{eq})} &= \delta\rho = \sum_i f_i, \\ \mathbf{j}^{(\mathrm{eq})} &= \mathbf{j} := (j_x, j_y) = \bar{\rho}\mathbf{u} = \sum_i f_i \mathbf{c}_i. \end{aligned} \tag{6}$$

For the *athermal* D2Q9 model in which the (internal) energy is *not* a conserved quantity, the equilibria for non-conserved moments are (Lallemand and Luo 2000):

$$\begin{aligned} e^{(\mathrm{eq})} &= -2\alpha_2\delta\rho + 3\left(j_x^2 + j_y^2\right), \\ \varepsilon^{(\mathrm{eq})} &= \delta\rho - 3\left(j_x^2 + j_y^2\right), \end{aligned} \tag{7a}$$

$$\mathbf{q}^{(\mathrm{eq})} = \left(q_x^{(\mathrm{eq})}, q_y^{(\mathrm{eq})}\right) = -\mathbf{j} = -(j_x, j_y), \tag{7b}$$

$$p_{xx}^{(\mathrm{eq})} = j_x^2 - j_y^2, \quad p_{xy}^{(\mathrm{eq})} = j_x j_y. \tag{7c}$$

With the above equilibria, the LBE system of equation (1) leads to the *incompressible* Navier–Stokes equations in the limit of small Mach number and large system size. If we choose $\alpha_2 = 1$ and set all the relaxation rates $\{s_i\}$ to a single value of $1/\tau$, i.e. $s_i = 1/\tau\ \forall i$, then the MRT–LBE reduces to the corresponding lattice Bhatnagar–Gross–Krook (BGK) equation (Bhatnagar *et al.* 1954, Chen *et al.* 1992, Qian *et al.* 1992).

The speed of sound for the model c_s and the shear viscosity ν and the bulk viscosity ζ are given by:

$$\begin{aligned} c_s^2 &= \frac{1}{3}(2 - \alpha_2), \quad \nu = \frac{1}{3}\left(\frac{1}{s_\nu} - \frac{1}{2}\right), \\ \zeta &= \frac{\alpha_2}{6}\left(\frac{1}{s_e} - \frac{1}{2}\right). \end{aligned} \tag{8}$$

It is apparent that when $\alpha_2 = 1$ and $s_\nu = s_e = 1/\tau$, we have $\zeta = \nu/2$ for the lattice BGK (LBGK) model. We should like to point out that this is one primary reason responsible for the numerical instability of the LBGK model, because for high Reynolds number flows ν is very small, and the bulk viscosity ζ is even smaller and thus insufficient to dissipate spurious density fluctuations in the system.

2.2 Boundary and initial conditions

The configuration for a 2D flow past a rotating circular cylinder of radius a near a plane wall is shown in figure 1. The computational domain is a rectangle of size $(X_u + X_d) \times (Y_h + a + H)$. We choose $Y_h = 20a$, $X_u = 20a$ and $X_d = 40a$ (Cheng *et al.* 2005). The cylinder radius a is equal to 40 lattice spacings. With $h = H/D$ between 0 and 2.5, the system size varies between 2400×840 and 2400×1040.

The boundary conditions are: a uniform inflow from the left, a free outflow at right, a free-slip at the top, and no-slip at the bottom and around the cylinder. The inflow boundary condition is given by

$$f_i = f_i^{(\mathrm{eq})}(\rho = \bar{\rho}, \mathbf{u} = (U, 0)). \tag{9}$$

A sufficiently large downstream domain is used to reduce the influence due to the outflow boundary conditions. At the outflow boundary, we use the equilibria with a fixed density $\bar{\rho}$ and the velocity is extrapolated from upstream (Chen *et al.* 1996).

The no-slip conditions in the LBE are realized with the bounce-back boundary conditions in which all particles colliding with a solid wall not reverse their momentum, but also gain the momentum imposed by the wall:

$$f_{\bar{i}} = f_i - 6w_i\rho\frac{\mathbf{c}_i \cdot \mathbf{U}_w}{c^2}, \tag{10}$$

where $f_{\bar{i}}$ is the distribution function of the velocity $\mathbf{c}_{\bar{i}} := -\mathbf{c}_i$, $\mathbf{U}_w$ is the wall velocity at the point where particle-wall collision takes place, and the coefficients $\{w_i\}$ for the D2Q9 model are: $w_0 = 4/9$, $w_{1,2,3,4} = 1/9$ and $w_{5,6,7,8} = 1/36$. With a fine resolution of $a = 40$, we can use the straight lattice lines to approximate the circular cylinder (zig-zag approximation), and find that this is indeed adequate for the present study.

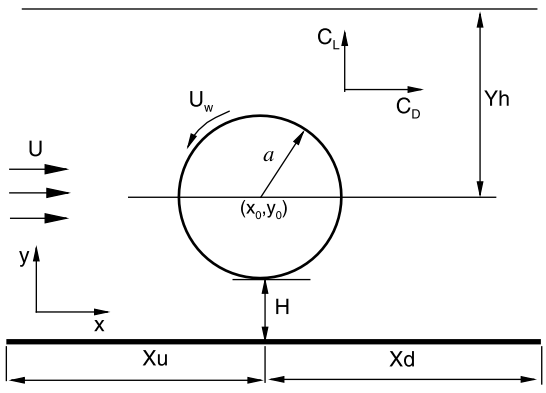

Figure 1. Schematic of flow configuration and coordinate.

In this paper, a potential flow past a circular cylinder is taken as the initial distribution of velocity:

$$U_0 = \left[1 - \frac{[(x_i - x_0)^2 - (y_i - y_0)^2]a^2}{[(x_i - x_0)^2 + (y_i - y_0)^2]^2}\right] U,$$

$$V_0 = -\frac{(x_i - x_0)(y_i - y_0)a^2}{[(x_i - x_0)^2 + (y_i - y_0)^2]^2} U, \qquad (11)$$

where x_0 and y_0 are the position of the cylinder center in the physical space, and

$$\mathbf{f} = \mathbf{f}^{(\mathrm{eq})}|^{t=0}_{\mathbf{u}_0=(U_0,V_0)} = \mathrm{M}\cdot\mathbf{m}^{(\mathrm{eq})}|^{t=0}_{\mathbf{u}_0=(U_0,V_0)}. \qquad (12)$$

Because the LBE is only valid for near incompressible flow, one usually maintains the Mach number $Ma := U/c_s < 0.3$ in practice. We use $U = 0.05$ throughout the simulations. Since $c_s = 1/\sqrt{3}$ is for the LBE model, $Ma = U/c_s \approx 0.09$.

The Reynolds number Re, lift (C_L) and drag (C_D) coefficients are defined as

$$Re = \frac{2aU}{\nu}, \quad C_\mathrm{L} = \frac{F_\mathrm{L}}{\bar{\rho}U^2 a}, \quad C_\mathrm{D} = \frac{F_\mathrm{D}}{\bar{\rho}U^2 a}, \qquad (13)$$

where F_L and F_D are the lift and drag forces exerted by the fluid on the cylinder, respectively. The relaxation rates s_8 and s_9 are determined by the viscosity ν (or Re): $s_8 = s_9 = 1/\tau = (3\nu + 1/2) = (6aU/Re + 1/2)$. Other relaxation rates are chosen as $s_2 = 1.6$, $s_3 = 1.2$ and $s_5 = s_7 = 1.5$ (Lallemand and Luo 2000).

2.3 Validation

The initial development of impulsively started flow around an isolated rotating circular cylinder has been studied both numerically and experimentally (Badr and Dennis 1985, Chen *et al.* 1993, Chew *et al.* 1995, Cheng *et al.* 2001). This flow is employed to validate the present method.

The flow past an isolated rotating circular cylinder at $\gamma = 0.5$ and $Re = 200$ is simulated using both the lattice BGK (LBGK) model and the MRT–LBE model. The streamlines around the cylinder at dimensionless times $t \in [2, 12]$ comparing the results of the LBGK and MRT–LBE models and that of Badr and Dennis (1985) are shown in figure 2. It can be observed in this figure that the streamline patterns generated by both the LBGK model and the MRT–LBE model agree well with the existing results generated by the conventional numerical method

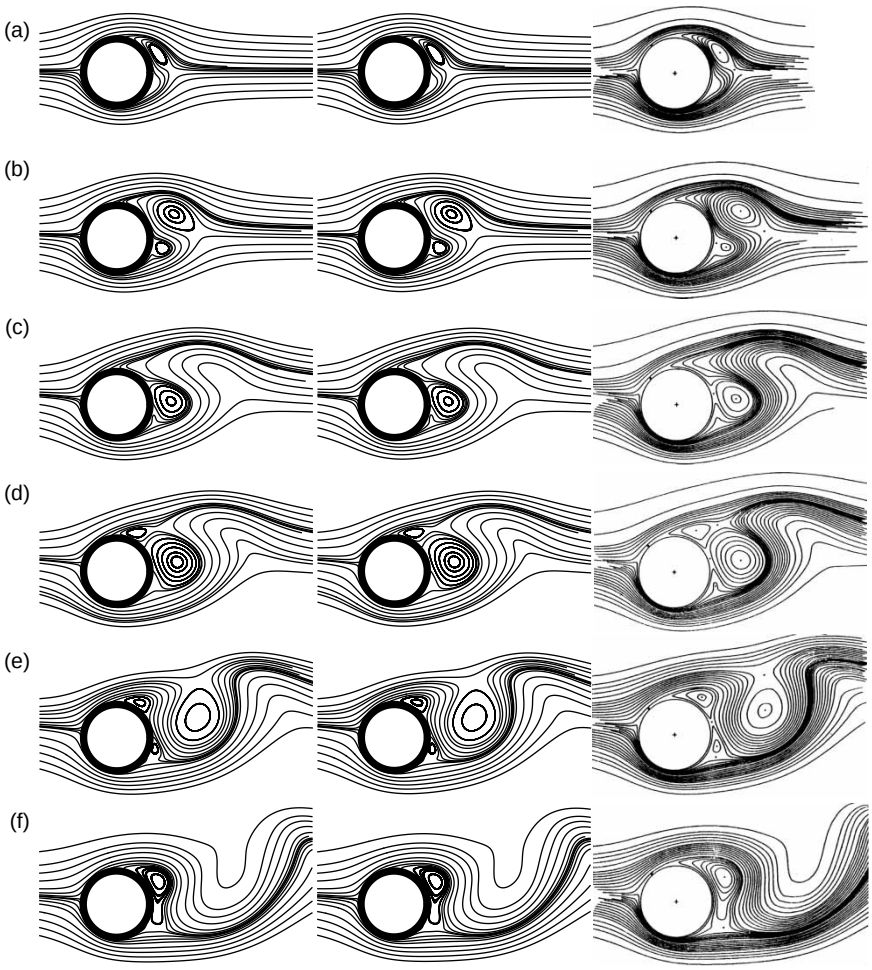

Figure 2. Comparison of the development of streamline patterns from the BGK (left), the MRT (center) models and the semi-analytical method (right) for $\gamma = 0.5$ at dimensionless times (a) $t = 2$, (b) $t = 4$, (c) $t = 7$, (d) $t = 8$, (e) $t = 10$ and (f) $t = 12$.

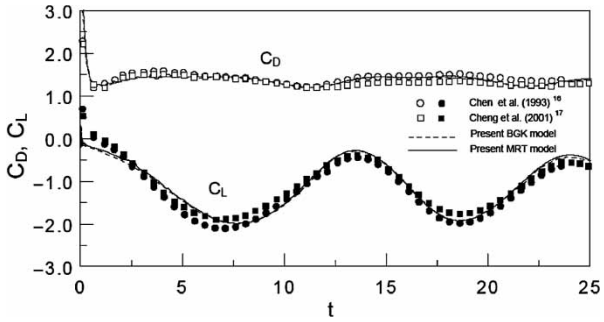

Figure 3. Comparison of time evolution of lift and drag coefficients from different methods for $Re = 200$ and $\gamma = 0.5$.

Badr and Dennis (1985). To further quantify the comparison between the present and the existing results, the time evolution of both the lift and drag coefficients is shown in figure 3. The time evolution of the lift and drag coefficients obtained by the different numerical methods also agree well with each other good over the range of time $t \in [0, 25]$ investigated previously (Chen *et al.* 1993, Cheng *et al.* 2001).

Although both the LBGK and MRT–LBE models yield good results on integrated quantities such as C_D and C_L, the instantaneous flow fields are difference. Figure 4 compares of vorticity contours from the LBGK and MRT–LBE models. The vorticity field computed by the LBGK model shows severe oscillation in the front of the cylinder, in contrast to the much smoother vorticity field obtained by using the MRT–LBE model. This clearly demonstrates the superiority of the MRT–LBE model over the popular LBGK model and this is the reason the MRT–LBE model is used in the present work.

3. Results and discussion

We next investigate the wall effect on the flow development behind a rotating circular cylinder at $Re = 200$ by varying the normalized gap $h := H/D$, where $D = 2a$ is the cylinder diameter. The typical wake patterns represented by the vorticity contours for $\gamma = 0.5$ and different gaps are shown in figure 5. These flow, exhibits the following features. When $h = 0.4$ (figure 5(a)), the negative vorticity shed from the upper side of the cylinder and the plane wall engulfs and neutralizes the positive vorticity shed from the lower side of the cylinder. There is no vortex shedding in the wake and the flow appears to be quasi-steady. This pattern does not change significantly when $h < 0.4$. The flow encounters a considerable resistance in passing through the viscous gap and is almost entirely reversed above the cylinder. As a consequence, the cylinder plus gap system behaves almost like a larger surface-mounted object. This phenomenon has also been observed experimentally by Bearman and Zdravkovich (1978), for flow past a stationary cylinder. However, compared to the flow past a stationary cylinder, the flow develops a larger recirculation zone behind the cylinder on the wall and a jet emanating from the gap for $\gamma > 0$ due to the rotation of the cylinder. When $h = 0.5$, the pattern of flow (figure 5(b)) is quite different from that of $h = 0.4$. A single vortex street appears in the wake slightly further away from the cylinder. When $h = 0.8$, the most striking feature about the flow develops: The appearance of alternating vortices shed from the upper and lower sides of the cylinder (figure 5(c)). As h increases to 1.0, the interaction between the wall and the vortex shedding weakens. It can be observed from figure 5(d), that vortices are shed alternatively, but the sizes of vortices shed from the upper and lower sides of the cylinder are still different. The former is fairly round whereas the latter tends to be elongated in near wake, and the vortex shed from the upper side of the cylinder moves faster downstream than that shed from the lower side of the cylinder. As the gap increases, the wall effect on the vortex shedding decreases further. When $h = 2.5$, the flow behind the cylinder is characterized by a Kármán vortex street of vortices in a regular alternating pattern, with a nearly constant distance between consecutive vortices. This suggest that when $h \geq 2.5$, the flow is almost free of the wall effects.

In order to gain more insight into the evolution process of vortex shedding in the near wake with different h, the vorticity contours at several time instants during one period T_v of vortex shedding are shown in figure 6 with $h = 0.5$ (left) and 1.0 (right). At some point in time, a vortex pair is already in the near wake and move downstream at an angle, as shown in figure 6(a) left, and this moment in time is

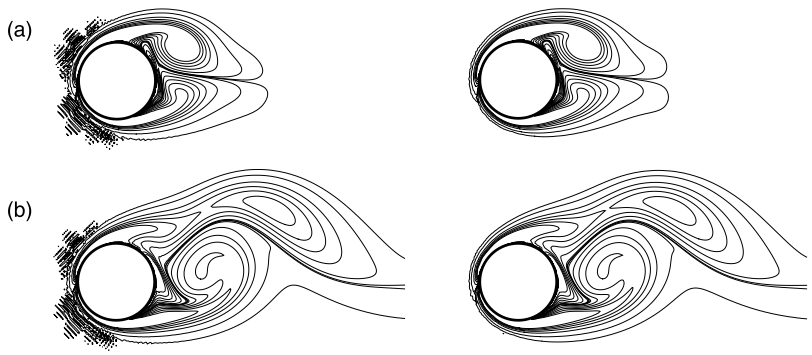

Figure 4. Comparison between instantaneous vorticity contours from the BGK (left) and MRT (right) models for $\gamma = 0.5$ at (a) $t = 4$ and (b) $t = 10$.

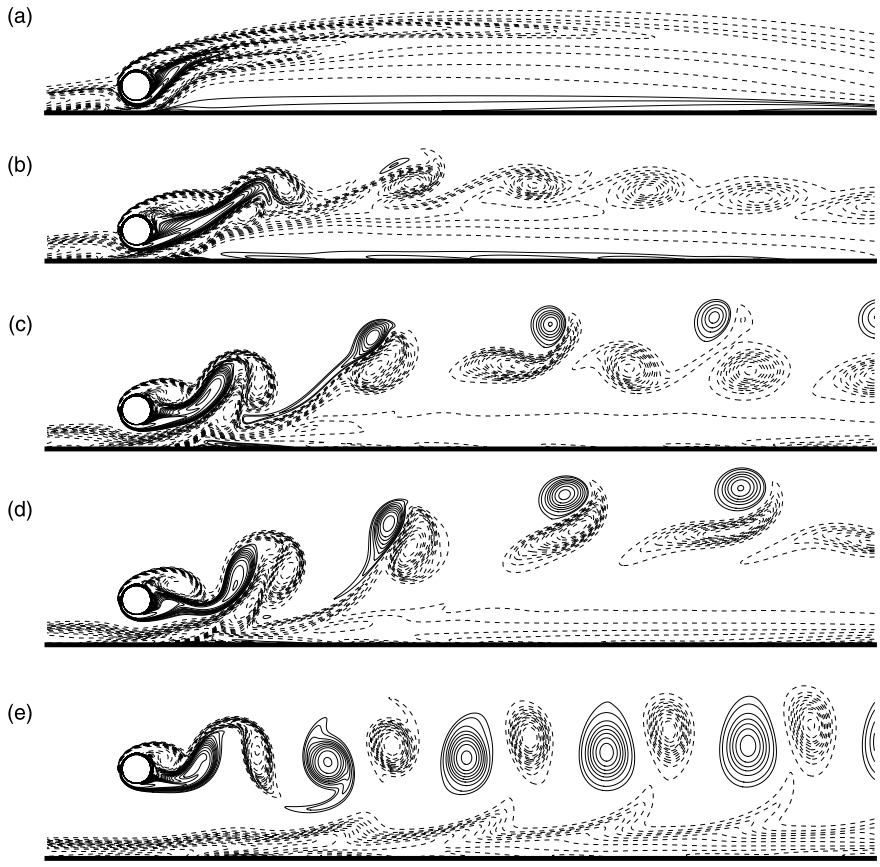

Figure 5. Instantaneous vorticity contours for $\gamma = 0.5$ at different gaps. (a) $h = 0.4$, (b) $h = 0.5$, (c) $h = 0.8$, (d) $h = 1.0$, and (e) $h = 2.5$. Solid and dash lines indicate the positive and negative vorticity, respectively.

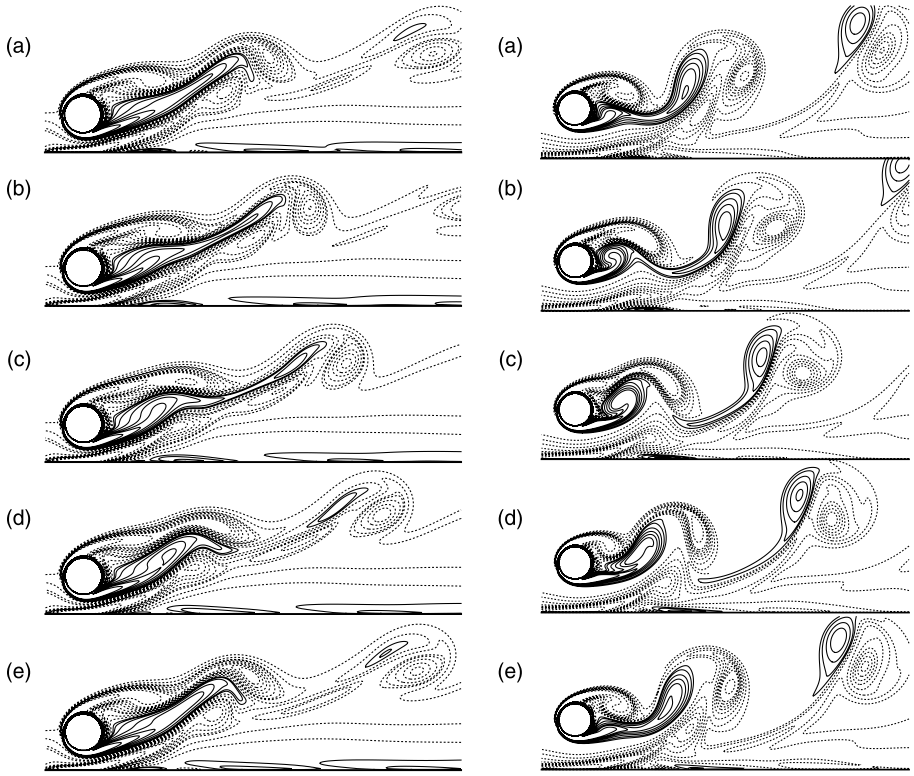

Figure 6. Vorticity contours during one cycle of vortex shedding for $\gamma = 0.5$, $h = 0.5$ (left) and $h = 1.0$ (right). (a) $t = T_0$, (b) $t = T_0 + T_v/5$, (c) $t = T_0 + 2T_v/5$, (d) $t = T_0 + 3T_v/5$ and (e) $t = T_0 + 4T_v/5$.

chosen as the initial starting time $t = T_0$. A vortex group is just being shed from the cylinder. They consist of a positive vortex generated from lower side of the cylinder and two negative vortices generated from upper side of the cylinder and the plane wall, respectively. The wall-side wake couples with the boundary layer vorticity of opposite sign on the plane wall while the actual wake is dominated by the vorticity shed from other side of the cylinder. The vortex separating from the lower side of the cylinder is stretched by the vorticity of opposite sign on the plane wall. Thus part of the vortex remains attached to the cylinder to from a quasi-steady attached wake while the farther part forms a very weak positive vortex. This vortex is oblate in shape and does not detach from the cylinder during time $t = T_0 + T_v/5$ to $t = T_0 + 2T_v/5$, with the period $T_v \approx 9.6$ in this case, corresponding to figure 6(b),(c), left, respectively. This is because, flow through the gap is suppressed so that the vortex shed from the lower side of the cylinder cannot be efficiently swept downstream by the free stream. As time increases, the positive vortex interacts with the forming vortex on the upper side of the cylinder (figure 6(c), left). Subsequently, they are swept together downstream at $t = T_0 + 3T_v/5$. The shapes of shedding vortices are a round vortex pair followed by a slender negative vortex (figure 6(d), left). The differences of the shedding vortex pair in size and strength are more pronounced as they travel downstream. It is observed from figure 6(e, left) that the core of positive vortex is more elongated, but it is still distinct in the near-wake. As the vortex travels downstream, it dissipates faster than these clockwise vortices, and eventually disappears so that only clockwise vortices remain and form a single vortex street in the wake slightly further away from the cylinder as shown in figure 5(b, left).

Figure 6 (right) shows the vorticity contours at five time instants during one cycle of vortex shedding at $h = 1.0$. A negative vortex appears on the upper side of the cylinder and a positive vortex begins to roll up on the lower side of the cylinder at $t = T_0$, while a vortex group is being formed by the vortices shed from cylinder and the vortex induced from the plane wall. After $t = T_0 + T_v/5$, the vortex formed on the plane wall first interacts with the vortex shed from the lower side of the cylinder (figure 6(b), right), right and then merges with the vortex shed from the upper side of the cylinder into a larger negative vortex (figure 6(c), right). At time $t = T_0 + 2T_v/5$ with $T_v \approx 9.2$, the rolling up positive vortex has assumed a rounded shape. During the period of $t = T_0 + 2T_v/5 - T_0 + 4T_\nu/5$, this vortex grows markedly in size and induces a vortex of opposite sign from the plane wall at time. It is clear that strength of the positive vortex shed from the lower side of the cylinder at $h = 1.0$ is stronger than that at $h = 0.5$. As time increases, a vortex group containing three vortices of uneven strength is formed and shed into the wake (figure 6(e), right). At $t = T_0 + 4T_v/5$, another positive vortex starts to roll up on the lower side of the cylinder. The evolution process repeats and one cycle of a vortex pair shedding takes about 10 dimensionless time-units.

The vorticity contours for $\gamma = 1.0$ with different h are shown in figure 7. The dependence of the flow pattern on h is found to be essentially the same as for $\gamma = 0.5$. That is, as the gap increases, the wake evolves from a quasi-steady flow to a Kármám vortex street. Comparing figure 7 with figure 5, however, one can find that the quasi-steady wake flow maintains till $h = 0.6$ when $\gamma = 1.0$, and the recirculation zone formed behind the cylinder on the

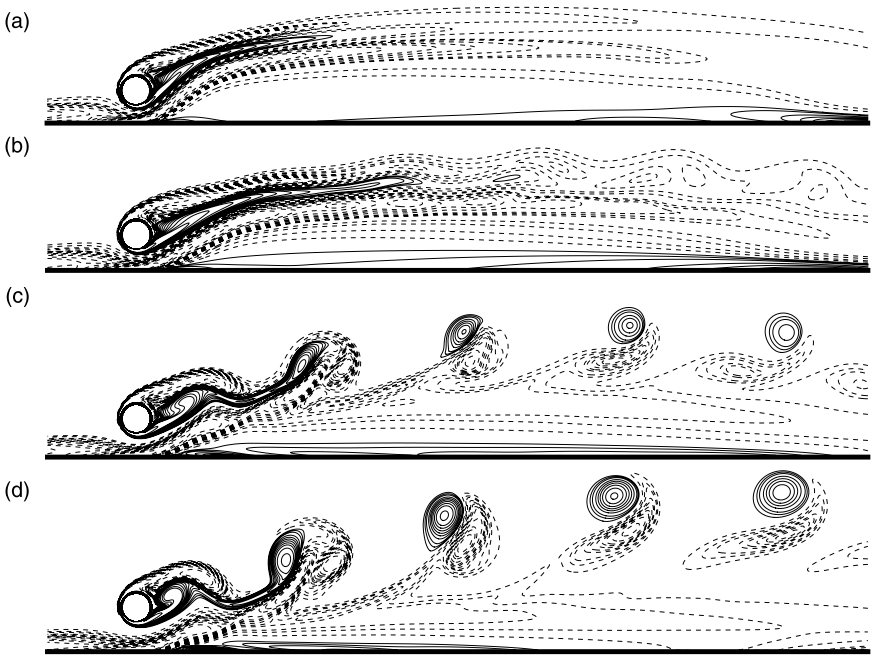

Figure 7. Instantaneous vorticity contours for $\gamma = 1.0$ with different h. (a) $h = 0.6$, (b) $h = 0.7$, (c) $h = 0.8$ and (d) $h = 1.0$.

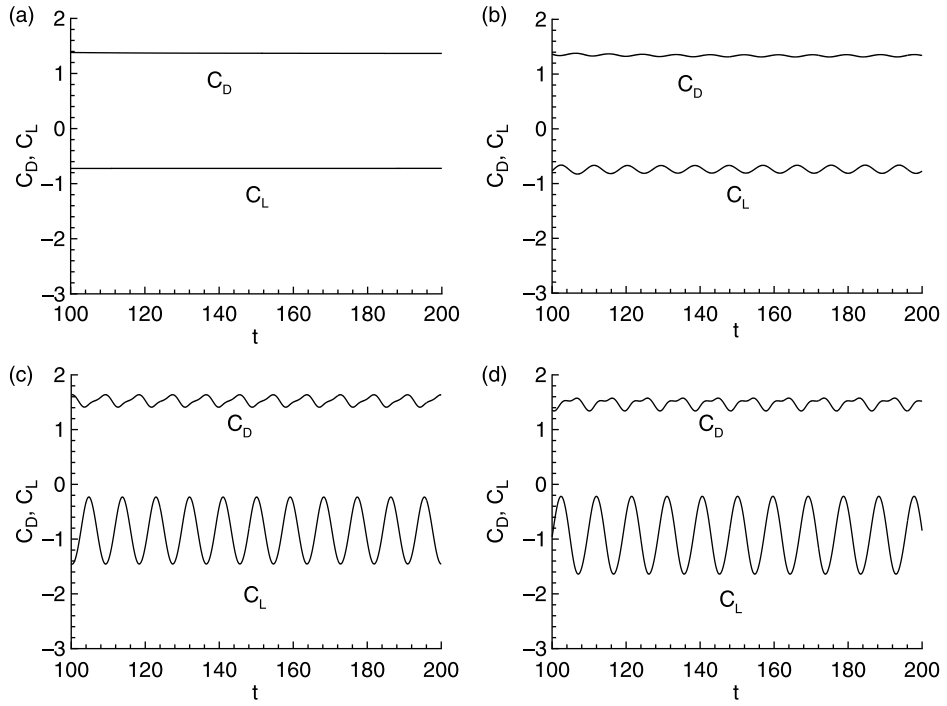

Figure 8. The time-histories of C_D and C_L for $\gamma = 0.5$ with different h. (a) $h = 0.4$, (b) $h = 0.5$, (c) $h = 1.0$ and (d) $h = 2.5$.

plane wall is larger than that of $\gamma = 0.5$. When $h = 0.7$, flow is highly unsteady, indicating that the higher the value of γ, the stronger the interaction between the wake and wall.

It is interesting to note how the lift and drag coefficients, C_L and C_D, vary with γ and h. The time histories of the lift and drag coefficients for $\gamma = 0.5$ are shown in figure 8. When $h = 0.4$, the lift and drag coefficients are constant because the flow is steady, as shown in figure 5(a). When $h = 0.5$, the lift and drag coefficients exhibit a time-dependent characteristic. This is due to the unstable transition, which occurs in the near wake. As h increases to 0.8, the variation of C_L and C_D with time shows a periodic fluctuation. The drag coefficient fluctuates with

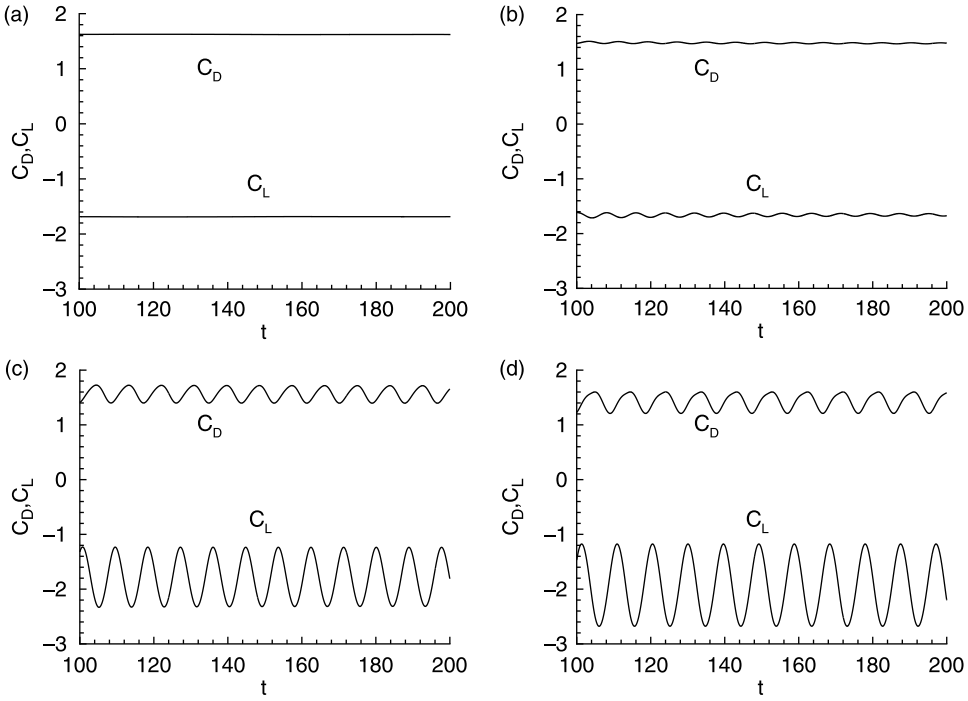

Figure 9. The time-histories of C_D and C_L for $\gamma = 1.0$ with different h. (a) $h = 0.6$, (b) $h = 0.7$, (c) $h = 1.0$ and (d) $h = 2.5$.

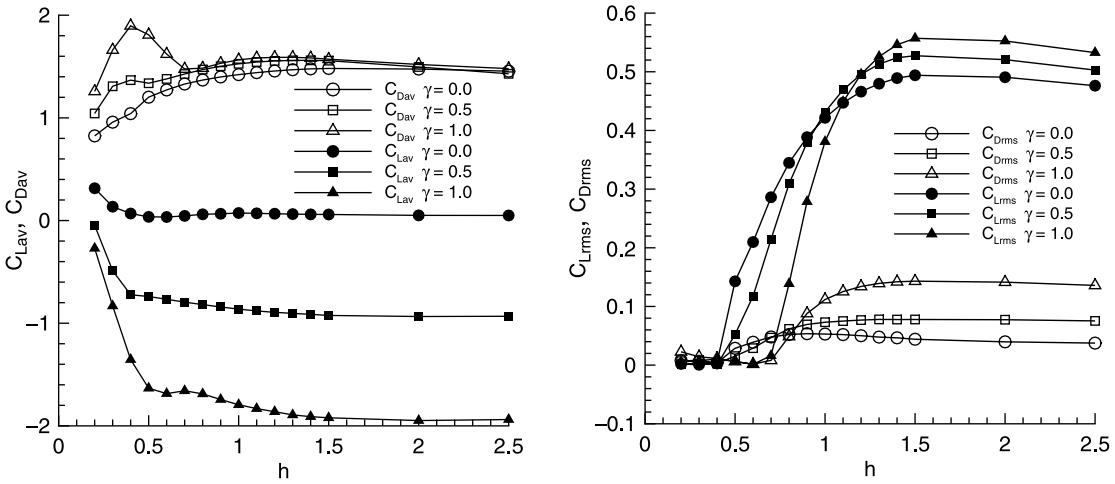

Figure 10. Variations of the mean (left) and root-mean-square (right) values of the lift and drag coefficients vs. h.

the same frequency of the lift coefficient. When $h = 1.0$, the lift coefficient shows a periodic fluctuation with a constant amplitude except the initial stage of the flow. It is clear that the periodic fluctuation is related to alternate vortex shedding as shown in figure 5(d). Compared to the case at $h = 0.5$, the amplitude of periodic fluctuation in the lift and drag coefficients remarkably increases at $h = 1.0$. The drag coefficient has a second harmonic component and one of the peaks of fluctuation is more pronounced than the other because the two oppositely signed vortices shed per cycle are different in strength.

When $h = 2.5$, similar to the case of $h = 1.0$, the second harmonic component in the drag coefficient becomes stronger, with one peak still weaker than the other. Overall, fluctuation amplitudes of C_D and C_L grow as h increases. The temporal behavior of the drag coefficient at $h = 2.5$ is rather similar to that for the flow past a rotating circular cylinder in an unbounded domain.

Figure 9 shows the time histories of the lift and drag coefficients for $\gamma = 1.0$. The curves of the lift and drag coefficients are still constants at $h = 0.6$, indicating that the larger the γ, the higher the h at which vortex shedding is suppressed. When $h = 0.7$, the unstable transition occurs in the near wake. As h increases, the fluctuation magnitude of the lift and drag coefficients clearly increases. This is similar to the case of $\gamma = 0.5$.

The variation of the mean values of the lift and drag coefficients, $\bar{C}_L$ and $\bar{C}_D$, with different h is shown in figure 10. An interesting feature to note is that the non-monotonic variation of the mean drag coefficient as a function of h with fixed γ. The mean draft coefficient $\bar{C}_D$ increases with h at first. With $\gamma = 0.5(1.0)$, $\bar{C}_D$ reaches a maximum of about 1.9 (1.4) at $h \approx 0.4$, then reduces to a local minimum of about 1.4 (1.36) at $h \approx 0.7(0.5)$, then increases slightly before decreasing to a constant value after $h > 1.5$. There is no such variation for the case of $\gamma = 0$. The mean lift coefficient $\bar{C}_L$ behaves differently. It decreases more rapidly with increase of h when $h < 0.5$, and then gradually decreases an constant value when $h > 1.5$.

Figure 10 also shows the variation of the root-mean-square (rms) values of the lift and drag coefficients, $\tilde{C}_L$ and $\tilde{C}_D$, as functions of h with different γ. When h is small, both $\tilde{C}_L$ and $\tilde{C}_D$ are close to zero because the flow is quasi-steady. As h increases beyond a certain value, which depends on γ, both $\tilde{C}_L$ and $\tilde{C}_D$ drastically increase, more so for $\tilde{C}_L$, to a maximum, and then remain nearly constant as h further increases. Clearly, the gap size h has a far stronger effect on the fluctuation of the lift, measured by $\tilde{C}_L$, than that of the drag.

4. Conclusion

Based on the numerical investigation conducted for $Re = 200$ with different gaps (h) and tangential speed (γ), the following conclusions can be made. For very small gaps, the gap flow is suppressed or extremely weak, and separation of the boundary layer occurs both upstream and downstream of the cylinder. There is no vortex shedding in the wake. The wake flow is stable. The larger the γ, the higher the h at which vortex shedding is suppressed.

When gap is smaller, the interaction between the shear layer on the plane wall and the growing positive vortex on the lower side of the cylinder causes the vortex pair in the near wake to move upward at an angle. The cores of positive vortices are elongated, but they are still distinct in the near-wake. As the positive vortices travel downstream, they dissipate faster than the negative ones.

As the gap increases, the interaction between the growing vortex and shear layer on the wall weakens. When the gap is greater than a certain value, there is no boundary layer separation on the wall, either upstream or downstream of the cylinder. A regular vortex street appears in the wake.

The present results suggest that the wall exerts a stronger influence on the lift and drag forces of a rotating cylinder than that of a stationary cylinder when the gap is small. Compared to the drag, the gap effect on the lift

force seems to be much larger, as observed in the present work.

It should be emphasized that the present study only considers a cylinder undergoing counter-clockwise rotation in an uniform flow from left to right. The phenomena would certainly be affected by the direction of the cylinder rotation. There could be a number of interesting wake flow features remained unexplored. Therefore, further investigations in details of the wall effect on the flow around a rotating circular cylinder is needed for a different rotation direction and Reynolds numbers.

The computational results not only reveal some basic features of shedding vortex in the near wake, but also demonstrate that the MRT model has better computational stability and produces smoother variation of the vorticity field.

References

Badr, H.M. and Dennis, S.C.R., Time-dependent viscous flow past an impulsively started rotating and translating circular cylinder. *J. Fluid Mech.*, 1985, **158**, 447–488.

Bearman, P.W. and Zdravkovich, M.M., Flow around a circular cylinder near a plane boundary. *J. Fluid Mech.*, 1978, **89**, 33–47.

Bhatnagar, P.L., Gross, E.P. and Krook, M., A model for collision processes in gases. I. Small amplitude processes in charged and neutral one-component systems. *Phys. Rev.*, 1954, **94**, 511–525.

Chen, H., Chen, S. and Matthaeus, H.W., Recovery of the Navier–Stokes equations using a lattice-gas Boltzmann method. *Phys. Rev. A*, 1992, **45**, R5339–R5342.

Chen, S., Martínez, D. and Mei, R., On boundary conditions in lattice Boltzmann methods. *Phys. Fluids*, 1996, **8**, 2527–2536.

Chen, Y.M., Ou, Y.R. and Pearlstein, A.J., Development of the wake behind a circular cylinder impulsively started into rotatory and rectilinear motion. *J. Fluid Mech.*, 1993, **253**, 449–484.

Cheng, M., Liu, G.R. and Lam, K.Y., Numerical simulation of flow past a rotationally oscillating cylinder. *Comput. Fluids*, 2001, **30**, 365–392.

Cheng, M., Tan, S.H.N. and Hung, K.C., Linear shear flow over a square cylinder at lower Reynolds number. *Phys. Fluids*, 2005, **17**, 078103.

Cheng, M., Tsuei, H.E. and Chow, K.L., Experimental study on flow interference phenomena of cylinder/cylinder and cylinder/plane arrangements. In *Flow-Induced Vibration*, edited by M.K. Au-Yang, pp. 173–184, 1994 (ASME: New York, NY).

Chew, Y.T., Cheng, M. and Luo, S.C., A numerical study of vortex shedding from a rotating circular cylinder by a hybrid vortex method. *J. Fluid Mech.*, 1995, **299**, 35–71.

d'Humières, D., Generalized lattice-Boltzmann equations. In *Rarefied gas dynamics: theory and simulations*, Prog. Astronaut. Aeronaut edited by B.D. Shizgal and D.P. Weave, **Vol. 159**, pp. 450–458, 1992 (AIAA: Washington DC).

d'Humières, D., Ginzburg, I., Krafczyk, M., Lallemand, P. and Luo, L.S., Multiple-relaxation-time lattice Boltzmann models in three-dimensions. *Philo. Trans. R. Soc. Lond. A*, 2002, **360**, 437–451.

Ginzbourg, I. and Adler, P.M., Boundary flow condition analysis for the three-dimensional lattice Boltzmann model. *J. Phys. II*, 1994, **4**, 191–214.

Ginzbourg, I. and d'Humières, D., Local second-order boundary methods for lattice Boltzmann models. *J. Stat. Phys.*, 1996, **84**(5/6), 927–971.

Ginzburg, I. and d'Humières, D., Multireflection boundary conditions for lattice Boltzmann models. *Phys. Rev. E*, 2003, **68**, 066614.

He, X. and Luo, L.S., Lattice Boltzmann model for the incompressible Navier–Stokes equation. *J. Stat. Phys.*, 1997, **88**, 927–944.

Lallemand, P. and Luo, L.S., Theory of the lattice Boltzmann method: Dispersion, dissipation, isotropy, Galilean invariance, and stability. *Phys. Rev. E*, 2000, **61**(6), 6546–6562.

Lallemand, P. and Luo, L.S., Lattice Boltzmann method for moving boundaries. *J. Comput. Phys.*, 2003, **184**, 406–421.

Pan, C., Luo, L.S. and Miller, C.T., An evaluation of lattice Boltzmann schemes for porous medium flow simulation, To appear in Comput. Fluids, 2005.

Prandtl, L., The Magnus effect and windpowered ships. *Naturwissenschaften*, 1925, **13**, 93–108.

Price, S.J., Sumner, D., Smith, J.G., Leong, K. and Paidoussis, M.P., Flow visualization around a circular cylinder near to a plane wall. *J. Fluid Struct.*, 2002, **16**, 175–191.

Qian, Y.H., d'Humières, D. and Lallemand, P., Lattice BGK models for Navier–Stokes equation. *Europhys. Lett.*, 1992, **17**, 479–484.

Sumer, B.M. and Fredsoe, J., *Hydrodynamics Around Cylindrical Structures*, 1997 (World Scientific: Singapore).

Taneda, S., Experimental investigation of vortex streets. *J. Phys. Soc. Jap.*, 1965, **20**, 1714–1721.

van Leer, B, Computational fluid dynamics: science or toolbox?, Technical report AIAA-2001–2520, AIAA, presented in 15th AIAA CFD Conference, June 11–14, 2001, Anaheim, CA. 2001.

Yu, D., Mei, R., Luo, L.S. and Shyy, W., Viscous flow computations with the method of lattice Boltzmann equation. *Prog. Aerospace Sci.*, 2003, **39**, 329–367.

Zdravkovich, M.M., Forces on a circular cylinder near a plane wall. *Appl. Ocean Res.*, 1985, **7**, 197–201.